

Negative-parity baryon spectra in quenched anisotropic lattice QCD

Y. Nemoto*,¹ N. Nakajima,² H. Matsufuru,¹ and H. Suganuma³

¹*Yukawa Institute for Theoretical Physics, Kyoto University, Kyoto 606-8502, Japan*

²*Center of Medical Information Science, Kochi Medical School, Kochi, 783-8505 Japan*

³*Faculty of Science, Tokyo Institute of Technology, Tokyo 152-8551, Japan*

We investigate the negative-parity baryon spectra in quenched lattice QCD. We employ the anisotropic lattice with standard Wilson gauge and $O(a)$ improved Wilson quark actions at three values of lattice spacings with renormalized anisotropy $\xi = a_\sigma/a_\tau = 4$, where a_σ and a_τ are spatial and temporal lattice spacings, respectively. The negative-parity baryons are measured with the parity projection. In particular, we pay much attention to the lowest $SU(3)$ flavor-singlet negative-parity baryon, which is assigned as the $\Lambda(1405)$ in the quark model. For the flavor octet and decuplet negative-parity baryons, the calculated masses are close to the experimental values of corresponding lowest-lying negative-parity baryons. In contrast, the flavor-singlet baryon is found to be about 1.7 GeV, which is much heavier than the $\Lambda(1405)$. Therefore, it is difficult to identify the $\Lambda(1405)$ to be the flavor-singlet three-quark state, which seems to support an interesting picture of the penta-quark ($udsq\bar{q}$) state or the $N\bar{K}$ molecule for the $\Lambda(1405)$.

PACS numbers: 12.38.Gc, 14.20.Gk, 14.20.Jn

I. INTRODUCTION

The lattice QCD simulation has become a powerful method to investigate hadron properties directly based on QCD. The spectroscopy of lowest-lying hadrons in the quenched approximation, i.e., without dynamical quark-loop effects, has been almost established, and reproduces their experimental values within 10 % deviations [1]. Extensive simulations including dynamical quarks are in progress and would give us detailed understanding of the spectra of these ground-state hadrons [2]. In contrast, several lattice studies on the excited-state hadrons have been started [3, 4, 5, 6, 7, 8, 9] very recently, and their calculations are far from established even at the quenched level. In this paper, using anisotropic lattice QCD, we investigate the low-lying negative-parity baryon spectra, particularly paying attention to the flavor-singlet baryon. Another purpose of this paper is to examine the correspondence between the flavor-singlet three-quark (3Q) state and the $\Lambda(1405)$.

In the context of the flavor-singlet baryon, the $\Lambda(1405)$ is known to be one of the most mysterious hadrons. The $\Lambda(1405)$ is the lightest negative-parity baryon, although it contains strangeness. Moreover, there are two physical interpretations on the $\Lambda(1405)$. From the viewpoint of the quark model, the $\Lambda(1405)$ is described as the flavor-singlet 3Q system. As another interpretation, the $\Lambda(1405)$ is an interesting candidate of the hadronic molecule such as the $N\bar{K}$ bound state with a large binding energy of about 30 MeV. We aim to clarify whether the $\Lambda(1405)$ can be explained as a flavor-singlet baryon in quenched lattice QCD.

Historically, excited-state baryons have been so far

mainly investigated within the framework of the non-relativistic quark model, in which baryons can be classified in terms of the spin-flavor $SU(6)$ symmetry. While the ground-state baryons have completely symmetric spin-flavor wave functions and form the 56-dimensional representation, the low-lying negative-parity baryons are parts of the $L = 1$ orbitally excited states and belong to the $SU(6)$ 70-dimensional representation. We summarize the classification of the $SU(6)$ symmetry and its assignment to experimentally observed baryons in Table I. Both the non-relativistic [10] and the semi-relativistic [11] quark models reproduce the negative-parity baryon spectra fairly well in the octet and the decuplet sectors [12]. Such success of the quark model implies that the constituent quark picture holds well and the gluonic excitation modes play a less important role. The potential form is being clarified with the recent lattice QCD calculations of the static 3Q potential [13, 14]. Furthermore, the large gluonic excitation energy [15] obtained with lattice QCD explains the reason why the quark potential model without such gluonic excitations well describes the hadron spectra.

Among the low-lying negative-parity baryons, the $\Lambda(1405)$ is an exception of such success of the quark potential model. In fact, the $\Lambda(1405)$ is much lighter than the lowest-lying non-strange negative-parity baryons, $N(1520)$ with $J^P = 3/2^-$ and $N(1535)$ with $J^P = 1/2^-$. There are two physical interpretations proposed for the $\Lambda(1405)$: an $SU(3)$ flavor-singlet 3Q state, and an $N\bar{K}$ bound state, i.e., a penta-quark (5Q) system. The simple quark model is based on the former picture, and it predicts that the $\Lambda(1405)$ and the $\Lambda(1520)$ with $J^P = 3/2^-$ are nearly degenerate [10, 11]. In this picture, the large mass difference between them is explained to originate from a large LS -force [16], but such a strong LS splitting is not observed in other baryon spectra, and therefore it seems difficult to reproduce the mass of the $\Lambda(1405)$ within the simple quark model.

*Present address: RIKEN BNL Research Center, BNL, Upton, NY 11973

Another interesting interpretation for the $\Lambda(1405)$ is the penta-quark (5Q) system or the $N\bar{K}$ bound state as a hadronic molecule [16, 17]. Note here that the $\Lambda(1405)$ lies about 30 MeV below the $N\bar{K}$ threshold, and this binding energy of about 30 MeV is rather large in comparison with about 2.2 MeV, that of the deuteron. If this picture holds true, the large binding energy between N and \bar{K} results in a significant role of the attractive effect for the \bar{K} put inside nuclei or nuclear matter. In this way, the study of such an exotic and strange baryon, the $\Lambda(1405)$, is important also for understanding of the manifestation of strangeness in the hyper-nuclei and the neutron stars.

The 3Q and the 5Q states, however, would mix in the real world. Therefore, a more realistic question would be as follows. Which is the dominant component of the $\Lambda(1405)$, the 3Q state or the 5Q state? We try to answer this question using lattice QCD simulations. In lattice QCD simulations, even if one chooses the operator as the 3Q or the 5Q state, it generally overlaps with both the states through the quark and anti-quark pair creation. In the quenched simulation, however, owing to the absence of dynamical quark-loop effects, such a mixing between 3Q and 5Q states are rather suppressed, which would enable us to investigate the properties of genuine 3Q and 5Q states in a separate manner.

In this paper, we focus on the 3Q state and investigate whether this picture can explain the mass of the $\Lambda(1405)$. Apparent discrepancy with the experimentally observed mass implies that the penta-quark state gives significant contribution to the physical $\Lambda(1405)$ state. In practice, lattice QCD results suffer from various systematic errors. It is therefore essential to compare the mass of the flavor-singlet 3Q state with other negative-parity baryon masses as well as with lowest-lying baryon masses.

It is also important to understand the gross structure of low-lying negative-parity baryon spectrum in relation to spontaneous chiral-symmetry breaking in QCD. If the chiral symmetry is restored, such as at high temperature and/or density, the masses of a baryon and its parity partner should be degenerate. Spontaneous chiral-symmetry breaking causes mass splitting between positive- and negative- parity baryons. It is important to study nonperturbatively negative-parity baryons in terms of the parity partners of the positive-parity ones.

Since the negative-parity baryons have relatively large masses, their correlators rapidly decrease in the Euclidean temporal direction. As a technical improvement, we adopt an anisotropic lattice where the temporal lattice spacing a_τ is finer than the spatial one, a_σ [18]. With the high resolution in the temporal direction, we can follow the change of the correlator in detail and specify the relevant region for extraction of the mass. Thus efficient measurements would be possible. This approach is efficient also for other correlators of heavy particles, such as the glueballs [19]. (The anisotropic lattice is extremely powerful for the study of the finite temperature QCD [19, 20, 21], where the temporal distance is severely

limited in the imaginary-time formalism.)

In this study, we adopt the standard Wilson plaquette gauge action and $O(a)$ improved Wilson quark action, for which the sizes of errors are rather well evaluated [22, 23]. The simulations are performed on the quenched anisotropic lattices with renormalized anisotropy $\xi = a_\sigma/a_\tau = 4$ at three lattice spacings in the range of $a_\sigma^{-1} \simeq 1\text{--}2$ GeV. For these lattices, the quark parameters were tuned and the light hadron spectrum was calculated in order to estimate the effects of uncertainties due to anisotropy on the spectrum [23].

This paper is organized as follows. In Section II, we summarize the anisotropic lattice actions used in this study. We show the numerical results on the negative-parity baryon in Section III, and discuss their physical consequences in Section IV. The last section is dedicated to the conclusion and perspective for further studies.

II. ANISOTROPIC LATTICE

We employ the standard Wilson plaquette gauge action and the $O(a)$ improved Wilson quark action on anisotropic lattices. We briefly summarize the anisotropic lattice action. The gauge field action takes the form

$$S_G = \beta \sum_x \left\{ \sum_{i>j=1}^3 \frac{1}{\gamma_G} \left[1 - \frac{1}{3} \text{ReTr} U_{ij}(x) \right] + \sum_{i=1}^3 \gamma_G \left[1 - \frac{1}{3} \text{ReTr} U_{i4}(x) \right] \right\} \quad (1)$$

with $\beta \equiv 2N_c/g^2$. Here, $U_{\mu\nu}$ denotes the parallel transport around a plaquette in μ - ν plane,

$$U_{\mu\nu}(x) = U_\mu(x)U_\nu(x + \hat{\mu})U_\mu^\dagger(x + \hat{\nu})U_\nu^\dagger(x). \quad (2)$$

The gluon field is represented with the link-variable as $U_\mu \simeq \exp(-iga_\mu A_\mu)$. The bare anisotropy γ_G coincides with the renormalized anisotropy $\xi = a_\sigma/a_\tau$ at the tree level.

Note here that the bare anisotropy is no longer the same as ξ due to the quantum effect, and one needs to measure ξ through some physical observables for each input value of γ_G . Although ξ is in general a function of gauge and quark parameters, (β, γ_G) and (κ, γ_F) respectively, on a quenched lattice, the calibrations of the gauge and quark actions can be performed separately. For the gauge action of the form (1), Klassen nonperturbatively obtained an expression of γ_G in terms of β and ξ with the accuracy better than 1% using the Wilson loops [22]. We adopt the same lattice actions as those in Ref.[23] which made use of the Klassen's result for the gauge action and also performed sufficient analysis for the quark actions as mentioned below.

For the Wilson type quark action, $O(a)$ improvement is significant in quantitative computation of hadron spectrum. Among several types of the anisotropic lattice

TABLE I: Quark model assignments for experimentally observed baryons in terms of the spin-flavor SU(6) basis [16].

$SU(6)$ rep.	$SU(3)_f$ rep.	J^P	$S = 0$	$S = -1, I = 0$	$S = -1, I = 1$	$S = -2$	$S = -3$
56 ($L = 0$)	2_8	$\frac{1}{2}^+$	$N(939)$	$\Lambda(1116)$	$\Sigma(1193)$	$\Xi(1318)$	
	$^4_{10}$	$\frac{3}{2}^+$	$\Delta(1232)$		$\Sigma(1385)$	$\Xi(1530)$	$\Omega(1672)$
70 ($L = 1$)	2_8	$\frac{1}{2}^-$	$N(1535)$	$\Lambda(1670)$	$\Sigma(1620)$	$\Xi(?)$	
		$\frac{3}{2}^-$	$N(1520)$	$\Lambda(1690)$	$\Sigma(1670)$	$\Xi(1820)$	
	4_8	$\frac{1}{2}^-$	$N(1650)$	$\Lambda(1800)$	$\Sigma(1750)$	$\Xi(?)$	
		$\frac{3}{2}^-$	$N(1700)$	$\Lambda(?)$	$\Sigma(?)$	$\Xi(?)$	
	$^2_{10}$	$\frac{1}{2}^-$	$N(1675)$	$\Lambda(1830)$	$\Sigma(1775)$	$\Xi(?)$	
		$\frac{3}{2}^-$	$\Delta(1620)$		$\Sigma(?)$	$\Xi(?)$	$\Omega(?)$
	2_1	$\frac{1}{2}^-$	$\Delta(1700)$		$\Sigma(?)$	$\Xi(?)$	$\Omega(?)$
		$\frac{3}{2}^-$			$\Lambda(1405)$		
		$\frac{3}{2}^-$		$\Lambda(1520)$			

quark action, we use the form proposed in Refs. [20, 23, 24]. As a merit of this form, the calibration with a good precision is rather easy in the light quark mass region, since the quark mass dependence is expected to be small there, as was numerically shown in Ref. [23].

The quark action is written as

$$S_F = \sum_{x,y} \bar{\psi}(x)K(x,y)\psi(y), \quad (3)$$

$$\begin{aligned}
K(x,y) = & \delta_{x,y} \\
& -\kappa_\tau \left\{ (1-\gamma_4)U_4(x)\delta_{x+\hat{4},y} + (1+\gamma_4)U_4^\dagger(x-\hat{4})\delta_{x-\hat{4},y} \right\} \\
& -\kappa_\sigma \sum_i \left\{ (r-\gamma_i)U_i(x)\delta_{x+\hat{i},y} + (r+\gamma_i)U_i^\dagger(x-\hat{i})\delta_{x-\hat{i},y} \right\} \\
& -\kappa_\sigma c_E \sum_i \sigma_{i4}F_{i4}\delta_{x,y} - r\kappa_\sigma c_B \sum_{i>j} \sigma_{ij}F_{ij}\delta_{x,y}, \quad (4)
\end{aligned}$$

where ψ denotes the anticommuting quark field, κ_σ and κ_τ the spatial and temporal hopping parameters, respectively, r the spatial Wilson parameter and c_E , c_B the clover coefficients. The field strength $F_{\mu\nu}$ is defined with the standard clover-leaf-type construction. In principle, for a given κ_σ , the four parameters $\kappa_\sigma/\kappa_\tau$, r , c_E and c_B should be tuned so that Lorentz symmetry is satisfied up to discretization errors of $O(a^2)$. Following Refs. [20, 23, 24], we set the spatial Wilson parameter as $r = 1/\xi$ and the clover coefficients as the tadpole-improved tree-level values, namely,

$$r = 1/\xi, \quad c_E = 1/u_\sigma u_\tau^2, \quad c_B = 1/u_\sigma^3. \quad (5)$$

To reduce large contribution from the tadpole diagram, the tadpole improvement [25] is applied by rescaling the link variables as $U_i(x) \rightarrow U_i(x)/u_\sigma$ and $U_4(x) \rightarrow U_4(x)/u_\tau$, with the mean-field values of the spatial and temporal link variables, u_σ and u_τ , respectively. This is equivalent to redefining the hopping parameters with the tadpole-improved ones (with tilde) through $\kappa_\sigma = \tilde{\kappa}_\sigma/u_\sigma$ and $\kappa_\tau = \tilde{\kappa}_\tau/u_\tau$. We define the anisotropy parameter γ_F as $\gamma_F \equiv \tilde{\kappa}_\tau/\tilde{\kappa}_\sigma$. This parameter in the action is to be

tuned nonperturbatively in the numerical simulation. It is convenient to define κ as

$$\frac{1}{\kappa} \equiv \frac{1}{\tilde{\kappa}_\sigma} - 2(\gamma_F + 3r - 4) = 2(m_0\gamma_F + 4), \quad (6)$$

where m_0 is the bare quark mass in temporal lattice units. This κ plays the same role as in the case of isotropic lattice, and is convenient to parameterize the quark mass together with the bare anisotropy γ_F .

The above action is constructed following the Fermilab approach [26], which proposes to tune the bare anisotropy parameter so that the rest mass and the kinetic mass equal each other. In practice, hadronic states are convenient to carry out this program. In Ref. [23], the bare anisotropy was tuned nonperturbatively using the relativistic dispersion relation of the pseudoscalar and vector mesons. The main result of Ref. [23] is as follows: They tuned γ_F in the quark mass range from the strange to charm quark masses with the accuracy better than 1%, and found that the tuned bare anisotropy, γ_F^* , is well fitted to the linear form in m_q^2 , where $m_q = (\kappa_c^{-1} - \kappa^{-1})/2\xi$ is naively defined quark mass. Then γ_F^* in the massless limit was obtained within 2% error, i.e., 1% as a statistical error and 1% as a systematic error in the form of fit in terms of m_q . Then, they computed the light hadron spectrum using the value of γ_F^* at the chiral limit, and observed the effect of uncertainty in γ_F^* on the spectrum for physical quark masses of the 1%-level. In the present study, we also treat the same quark mass region and therefore adopt the value of γ_F^* in the chiral limit. The precision of 2% error in γ_F^* is sufficient for the present purpose.

As was pointed out in Refs. [20, 23], with the choice $r = 1/\xi$, the action (4) leads to a smaller spatial Wilson term for a larger anisotropy ξ . Since the negative-parity baryons measured in this paper are the lowest state of the parity projected baryon correlators, the statements in Ref. [23] for light hadrons also hold in our calculation. Even for the coarsest lattice in our calculation, the cutoff $a_\tau^{-1} \simeq 4.0$ GeV seems sufficiently large to avoid the artificial excitation due to the doublers in the ground-state

signals. At least, the finest lattice with $a_\tau^{-1} \simeq 8$ GeV would be sufficiently large to avoid the doubler effect.

III. NUMERICAL SIMULATION

A. Lattice setup

The numerical simulation is performed on the same lattices as in Ref. [23]. Here, we briefly summarize the fundamental parameters and physical quantities. We use the three anisotropic lattices with the renormalized anisotropy $\xi = 4$, at the quenched level. The statistical uncertainties are, otherwise noted, estimated by the Jackknife method with appropriate binning.

The lattice sizes and parameters in generating the gauge field configurations are listed in Table II. The spatial lattice scales a_σ^{-1} roughly cover 1–2 GeV. The values of bare gluonic anisotropy γ_G are chosen according to the result by Klassen [22]. The uncertainty of his expression is of the order of 1%, and in the following analysis we do not include this uncertainty in the quoted statistical errors. The gauge configurations are separated by 2000 (1000) pseudo-heat-bath sweeps, after 20000 (10000) thermalization sweeps at $\beta=5.95$ and 6.10 (5.75). The configurations are fixed to the Coulomb gauge, which is convenient in applying the smearing of hadron operators.

The mean-field values of link variables are determined on the smaller lattices with half size in temporal extent and otherwise with the same parameters for $\beta = 5.75$ and 5.95, while at $\beta = 6.10$ the lattice size is $16^3 \times 64$. The mean-field values, u_σ and u_τ , are obtained as the averages of the link variables in the Landau gauge, where the mean-field values are self-consistently used in the fixing condition [20]. In a study of hadron spectrum, it is convenient to define the lattice scales through a hadronic quantity. We determine a_σ^{-1} through the K^* meson mass, $m_{K^*} = 893.9$ MeV (isospin averaged). The procedure is the same as in Ref. [23], while with larger statistics. The result is quoted in Table II as $a_\sigma^{-1}(m_{K^*})$.

The quark parameters are listed in Table III. These hopping parameters roughly cover the quark masses $m_q \simeq m_s - 2m_s$. The numbers of configurations are larger than those of the hadronic spectroscopy in Ref. [23]. As already noted in the previous section, the values of γ_F and κ_c are taken from the result of Ref. [23]. Although the uncertainty of 2% level is associated with the values of γ_F , the quoted errors of hadron masses in the following analysis do not include this uncertainty. According to Ref. [23], this uncertainty in the physical masses of vector mesons and positive-parity baryons are at most of order of 1%. For the negative-parity baryon masses, the effect is expected to be similar amount and not significant compared with the present level of statistical error. Therefore, this effect can be negligible in our calculation.

As described later, we first extrapolate the vector meson mass linearly in the pseudoscalar meson mass squared

to the point at which the ratio of these meson masses are equal to the physical value, m_{K^*}/m_K . At this point, aforementioned lattice scale is determined. The physical (u , d) and s quark masses are determined through the π and K meson masses, $m_\pi^\pm = 139.6$ MeV and $m_K = 495.7$ MeV (isospin averaged), respectively.

B. Baryon correlators

We measure the correlators in pseudoscalar and vector meson channels and octet (Σ and Λ types), decuplet and singlet channels of SU(3) flavor representation of baryons. As listed in Table IV, we use the standard meson and baryon operators which have the same quantum numbers as the corresponding baryons and survive in the non-relativistic limit. It is known that there are mainly two ways to choose the baryon operator. One is the operator taken here, $(q^T C \gamma_5 q)q$, and the other is of the form $(q^T C q) \gamma_5 q$. There are two reasons why we take the former. It is well-known that the former operators strongly couple to the the ground-state baryons and reproduce experimental values well. Therefore, it is suitable for investigation of the parity partner of the ground state baryons. Furthermore, the recent lattice calculation shows that these two operators give the similar results for the negative-parity baryon spectrum while the latter is more noisy [5].

For baryons, two of three quark masses are taken to be the same value as specified by the hopping parameter κ_1 , and the other quark mass is specified by κ_2 . This corresponds to taking the same value for u, d current quark masses as $m_u = m_d \equiv m_n$. Then, the baryon masses are expressed as the function of two masses m_1 and m_2 , or equivalently of κ_1 and κ_2 , like $m_B(\kappa_1, \kappa_2)$. In the source operator, each quark field is smeared with the Gaussian function of width $\simeq 0.4$ fm.

At large t (and large $N_t - t$), the baryon correlators are represented as

$$\begin{aligned} G_B(t) &\equiv \sum_{\vec{x}} \langle B(\vec{x}, t) \bar{B}(\vec{x}, 0) \rangle \\ &= (1 + \gamma_4) \left[c_{B^+} \cdot e^{-tm_{B^+}} + b c_{B^-} \cdot e^{-(N_t-t)m_{B^-}} \right] \\ &\quad + (1 - \gamma_4) \left[b c_{B^+} \cdot e^{-(N_t-t)m_{B^+}} + c_{B^-} \cdot e^{-tm_{B^-}} \right], \quad (7) \end{aligned}$$

where $b = +1$ and -1 for the periodic and antiperiodic temporal boundary conditions for the quark fields. Since we adopt the standard Dirac representation for γ matrices, the upper and lower two components correspond to the first and second contributions of Eq. (7).

Combining the parity-projected correlators under two boundary conditions, one can single out the positive- and negative-parity baryon states with corresponding masses m_{B^+} and m_{B^-} , respectively, without contributions from the backward propagating parity partners. In practical simulation, however, we take a sufficient temporal extent so that we can observe an enough range of plateau in

TABLE II: Lattice parameters in the gluon sector. The scale $a_\sigma^{-1}(m_{K^*})$ is determined from the K^* meson mass. The mean-field values are defined in the Landau gauge. The statistical uncertainty of u_τ is less than the last digit. The details for these parameters are described in [23].

β	γ_G	size	u_σ	u_τ	$a_\sigma^{-1}(m_{K^*})$ [GeV]
5.75	3.072	$12^3 \times 96$	0.7620(2)	0.9871	1.034(6)
5.95	3.1586	$16^3 \times 128$	0.7917(1)	0.9891	1.499(9)
6.10	3.2108	$20^3 \times 160$	0.8059(1)	0.9901	1.871(14)

TABLE III: Lattice parameters in the quark sector. The values of γ_F and κ_c are taken from Ref. [23].

β	γ_F	κ_c	N_{conf}	values of κ
5.75	3.909	0.12640(5)	400	0.1240, 0.1230, 0.1220, 0.1210
5.95	4.016	0.12592(6)	400	0.1245, 0.1240, 0.1235, 0.1230
6.10	4.034	0.12558(4)	400	0.1245, 0.1240, 0.1235, 0.1230

effective mass plot for extraction of mass in each parity channel, and hence there is no advantage in computing correlators under two boundary conditions except for the reduction of statistical fluctuation. We obtain the baryon correlators at $\beta = 5.75$ under two boundary conditions, and compare the statistical fluctuations in the parity-projected correlator and in not projected one. We conclude that it is not worth doubling the computational cost and hence adopt only the periodic boundary condition hereafter. Instead, at each β we obtain the correlators with the source at $t = N_t/2$ in addition to ones with the source at $t = 0$, and average them. This is efficient to reduce the statistical errors for limited number of configurations.

C. lattice QCD results for hadron masses

Fig. 1 shows the effective mass plots for the baryon correlators at $\beta = 6.10$. The effective mass is defined without considering the contribution of the associated parity partner propagating backward from the source at $t = N_t$,

$$m_{\text{eff}} = \ln \left(\frac{G_B(t)}{G_B(t+1)} \right). \quad (8)$$

We observe that in the region where the effective mass exhibits a plateau, the contribution of parity partner is sufficiently small. In particular for the negative-parity baryon channels, fine temporal lattice spacing seems to be helpful to specify the region in which the ground state dominates.

The meson correlator is fitted to the single hyperbolic cosine form and analyzed independently of Ref. [23]. The results are shown in Fig. 2. and consistent with Ref. [23]. For the baryons, we fit the data to a single exponential form. The result is listed in Tables V, VI and VII.

Following Ref. [23], we extrapolate the hadron masses to the chiral limit in terms of the pseudoscalar meson

mass squared, instead of $1/\kappa$. The assumed relation between PS meson mass and quark mass is

$$m_{PS}^2(m_1, m_2) = B \cdot (m_1 + m_2), \quad (9)$$

then for the degenerate quark masses, $m_1 = m_2$, $m_{PS}^2 = 2Bm_1$ holds. Instead of m_i ($i=1,2$), one can extrapolate other hadron masses in term of $m_{PS}(m_i, m_i)^2$ to the chiral limit.

In our calculation for baryons, two of quark masses are taken to be the same value, m_1 , and the other quark mass m_2 is taken to be an independent value. Then, the baryon masses are expressed as the function of m_1 and m_2 like $m_B(m_1, m_2)$, and therefore they are to be depicted on the (m_1, m_2) plane. However, the result for the baryon masses seem to be well described with the linear relation,

$$m_B(m_1, m_2, m_3) = m_B(0, 0, 0) + B_B \cdot (2m_1 + m_2). \quad (10)$$

Therefore, we fit the baryon mass data to the linear form in the sum of corresponding PS meson masses squared. The vector meson is also fitted to a linear function in $m_1 + m_2$.

Note here that, in quenched QCD, a non-analyticity appears in the chiral extrapolation near the chiral limit [27]. For nucleons, it is reported that the departure from the simple chiral extrapolation is observed for $m_\pi < 400$ MeV [28]. Although we have to keep this effect in our mind, we do not argue it here because there is no distinct behavior for both the positive- and negative-parity baryons in our calculation with $m_\pi > 600$ MeV.

The results of fits for baryons are shown in Fig. 3 for each lattice. The horizontal axis is the averaged pseudoscalar meson mass squared,

$$\langle m_{PS}^2(m_i) \rangle = \frac{1}{N_q} \sum_{i=1}^{N_q} m_{PS}^2(m_i, m_i) = \frac{1}{N_q} \sum_{i=1}^{N_q} 2Bm_i \quad (11)$$

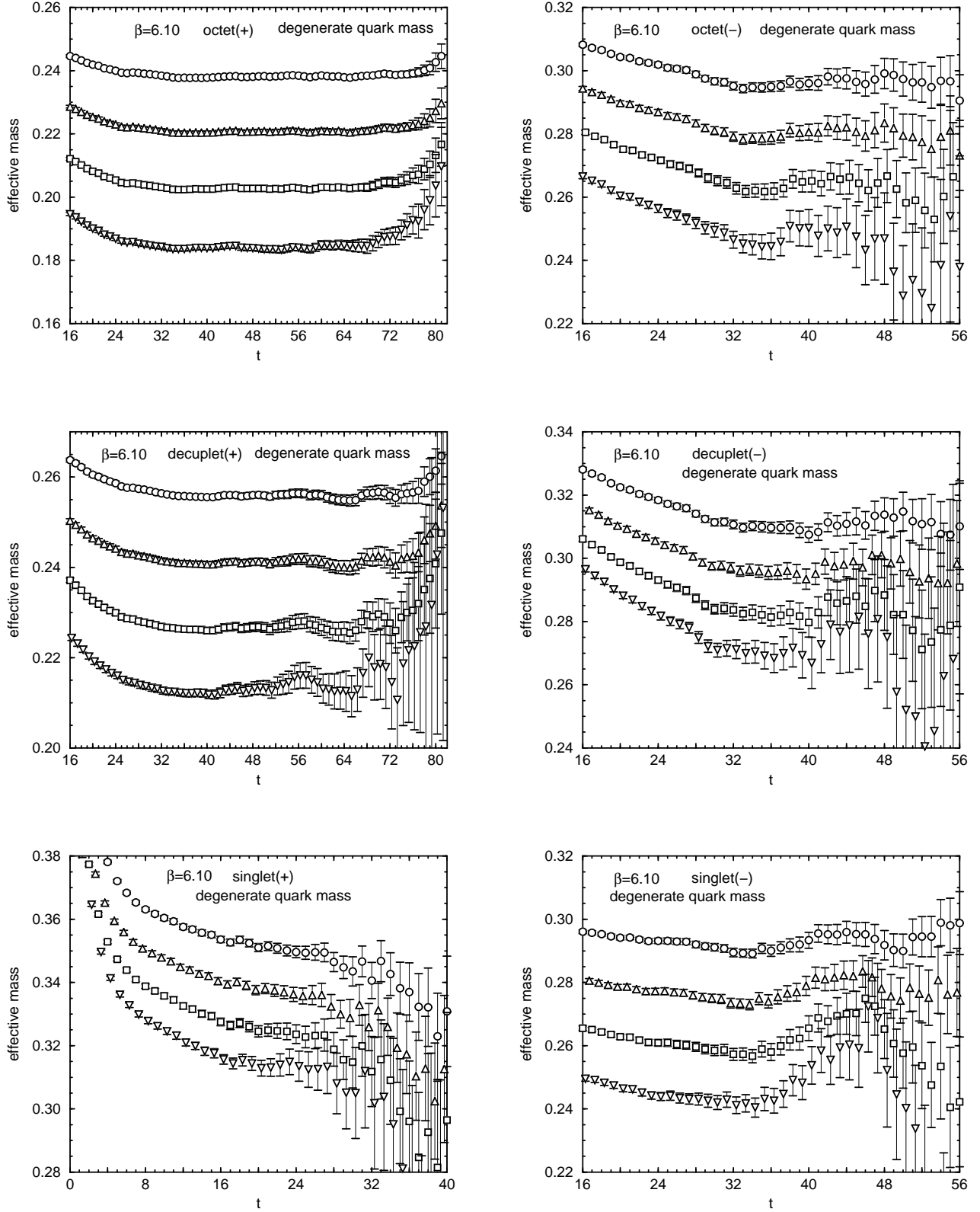


FIG. 1: Effective mass plots for octet, decuplet and singlet baryon correlators with degenerate quark masses at $\beta = 6.10$. The symbols correspond to $\kappa = 0.1230, 0.1235, 0.1240$ and 0.1245 from top to bottom in each figure. The left figures are for the positive-parity baryons and the right for the negative-parity ones.

TABLE IV: Typical interpolating operators for various hadrons. For baryons, the contraction with the color index is omitted. C denotes the charge conjugate matrix.

Meson	Pseudoscalar	$M(K) = \bar{s}\gamma_5 u$
	Vector	$M_k(K^*) = \bar{s}\gamma_k u$
Baryon	Octet	$B_\alpha(\Sigma^0) = (C\gamma_5)_{\beta\gamma}[u_\alpha(d_\beta s_\gamma - s_\beta d_\gamma) - d_\alpha(s_\beta u_\gamma - u_\beta s_\gamma)]$
	Octet (Λ)	$B_\alpha(\Lambda) = (C\gamma_5)_{\beta\gamma}[u_\alpha(d_\beta s_\gamma - s_\beta d_\gamma) + d_\alpha(s_\beta u_\gamma - u_\beta s_\gamma) - 2s_\alpha(u_\beta d_\gamma - d_\beta u_\gamma)]$
	Singlet	$B_\alpha(\Lambda_1) = (C\gamma_5)_{\beta\gamma}[u_\alpha(d_\beta s_\gamma - s_\beta d_\gamma) + d_\alpha(s_\beta u_\gamma - u_\beta s_\gamma) + s_\alpha(u_\beta d_\gamma - d_\beta u_\gamma)]$
	Decuplet	$B_{\alpha k}(\Sigma^{*0}) = (C\gamma_k)_{\beta\gamma}[u_\alpha(d_\beta s_\gamma + s_\beta d_\gamma) + d_\alpha(s_\beta u_\gamma + u_\beta s_\gamma) + s_\alpha(u_\beta d_\gamma + d_\beta u_\gamma)]$

TABLE V: Baryon spectrum at $\beta = 5.75$ in the temporal lattice unit. When quark masses are degenerate as $\kappa_1 = \kappa_2$, the Σ -type and the Λ -type octet baryon correlators become identical.

		Positive-parity baryons				Negative-parity baryons			
κ_1	κ_2	$m_{\text{oct}(\Sigma)}$	$m_{\text{oct}(\Lambda)}$	m_{sing}	m_{dec}	$m_{\text{oct}(\Sigma)}$	$m_{\text{oct}(\Lambda)}$	m_{sing}	m_{dec}
0.1210	0.1210	0.4281(9)	0.4281(9)	0.6426(56)	0.4606(16)	0.5443(52)	0.5443(52)	0.5355(30)	0.5630(54)
0.1210	0.1220	0.4171(10)	0.4186(10)	0.6349(59)	0.4518(17)	0.5355(56)	0.5356(57)	0.5265(32)	0.5548(59)
0.1210	0.1230	0.4059(10)	0.4091(10)	0.6267(64)	0.4433(19)	0.5271(61)	0.5270(64)	0.5175(34)	0.5467(66)
0.1210	0.1240	0.3946(11)	0.3998(11)	0.6184(69)	0.4352(21)	0.5189(68)	0.5178(78)	0.5089(37)	0.5386(78)
0.1220	0.1210	0.4083(10)	0.4066(10)	0.6275(63)	0.4430(19)	0.5269(61)	0.5269(60)	0.5173(33)	0.5465(65)
0.1220	0.1220	0.3970(11)	0.3970(11)	0.6206(68)	0.4341(20)	0.5181(66)	0.5181(66)	0.5080(35)	0.5382(71)
0.1220	0.1230	0.3855(11)	0.3874(11)	0.6132(74)	0.4256(22)	0.5095(73)	0.5091(75)	0.4989(38)	0.5300(79)
0.1220	0.1240	0.3737(12)	0.3780(12)	0.6055(81)	0.4176(25)	0.5012(82)	0.4994(90)	0.4899(41)	0.5217(93)
0.1230	0.1210	0.3885(11)	0.3845(11)	0.6116(74)	0.4259(22)	0.5091(77)	0.5099(74)	0.4990(38)	0.5302(81)
0.1230	0.1220	0.3769(12)	0.3747(12)	0.6063(81)	0.4171(24)	0.5001(83)	0.5008(81)	0.4895(41)	0.5218(89)
0.1230	0.1230	0.3650(12)	0.3650(12)	0.6004(89)	0.4085(27)	0.4913(92)	0.4913(92)	0.4801(44)	0.513(10)
0.1230	0.1240	0.3527(13)	0.3554(13)	0.5939(99)	0.4004(32)	0.483(11)	0.481(11)	0.4707(48)	0.505(12)
0.1240	0.1210	0.3689(13)	0.3612(13)	0.5936(89)	0.4099(30)	0.489(11)	0.4928(98)	0.4805(46)	0.514(11)
0.1240	0.1220	0.3569(14)	0.3512(14)	0.591(10)	0.4010(33)	0.480(12)	0.483(11)	0.4708(49)	0.505(12)
0.1240	0.1230	0.3445(15)	0.3414(15)	0.588(11)	0.3922(37)	0.470(13)	0.473(12)	0.4610(53)	0.496(14)
0.1240	0.1240	0.3317(16)	0.3317(16)	0.585(13)	0.3838(45)	0.460(15)	0.460(15)	0.4509(58)	0.486(16)
fit range		24–40	24–40	12–20	28–40	20–32	20–32	16–24	20–32

with $N_q = 3$ for baryons. The results of fits are displayed as the solid lines in these figures. The linear relation seems to hold well.

As stated in Section III, we determine the scale a_τ^{-1} through the K^* meson mass. The physical (u , d) and s quark masses are determined with the π and K meson masses. The scales of the vertical and horizontal axes in Fig. 3 are set in this way. The corresponding hadron masses for the physical quark masses are listed in Table VIII. These results for the meson masses and positive-parity baryon masses are consistent with those obtained in Ref. [23].

D. Systematic errors

Finally before discussing physical implications of our numerical results, we briefly comment on the systematic uncertainties.

- *Anisotropy (calibration)*

According to the detailed inspection given in Ref. [23], the 2% uncertainty in γ_F causes uncertainties in hadron masses at 1% level. Although the effect of uncertainty coming from anisotropy on the negative parity baryon masses is unknown, its size is expected to be the same level as for the positive-parity baryons and smaller than their statistical errors. Therefore, we do not perform a detailed analysis of the calibration uncertainty here. The uncertainty in γ_G , the gluonic anisotropy parameter, is also kept within 1% level, and hence for the same reason as for γ_F , we do not argue its effect on the negative-parity baryon masses.

- *Finite volume effects*

Since the excited baryons may have larger spatial extent than the ground state baryons, they may seriously suffer from the finite size effects. Our present three lattices, however, have almost

TABLE VI: The same results as Table V for $\beta = 5.95$.

		Positive-parity baryons				Negative-parity baryons			
κ_1	κ_2	$m_{\text{oct}(\Sigma)}$	$m_{\text{oct}(\Lambda)}$	m_{sing}	m_{dec}	$m_{\text{oct}(\Sigma)}$	$m_{\text{oct}(\Lambda)}$	m_{sing}	m_{dec}
0.1230	0.1230	0.2785(7)	0.2785(7)	0.4279(27)	0.3041(10)	0.3537(28)	0.3537(28)	0.3460(32)	0.3771(36)
0.1230	0.1235	0.2722(7)	0.2732(7)	0.4240(28)	0.2993(10)	0.3482(30)	0.3487(30)	0.3407(33)	0.3728(39)
0.1230	0.1240	0.2658(7)	0.2680(8)	0.4202(30)	0.2945(11)	0.3428(32)	0.3441(34)	0.3355(36)	0.3690(43)
0.1230	0.1245	0.2592(8)	0.2628(8)	0.4165(34)	0.2899(12)	0.3374(35)	0.3406(40)	0.3306(40)	0.3661(48)
0.1235	0.1230	0.2675(7)	0.2664(7)	0.4203(30)	0.2944(11)	0.3434(33)	0.3430(32)	0.3354(35)	0.3686(42)
0.1235	0.1235	0.2610(8)	0.2610(8)	0.4168(33)	0.2896(12)	0.3378(35)	0.3378(35)	0.3299(38)	0.3643(45)
0.1235	0.1240	0.2545(8)	0.2557(8)	0.4133(36)	0.2848(12)	0.3322(38)	0.3330(39)	0.3246(41)	0.3604(49)
0.1235	0.1245	0.2477(8)	0.2504(9)	0.4099(40)	0.2801(14)	0.3268(42)	0.3291(46)	0.3195(45)	0.3575(56)
0.1240	0.1230	0.2564(8)	0.2538(8)	0.4129(36)	0.2849(13)	0.3332(40)	0.3324(38)	0.3247(41)	0.3608(50)
0.1240	0.1235	0.2498(8)	0.2484(8)	0.4099(40)	0.2800(13)	0.3275(42)	0.3270(41)	0.3192(44)	0.3565(54)
0.1240	0.1240	0.2430(9)	0.2430(9)	0.4070(44)	0.2751(14)	0.3218(46)	0.3218(46)	0.3136(48)	0.3527(60)
0.1240	0.1245	0.2359(9)	0.2375(10)	0.4041(50)	0.2704(16)	0.3162(52)	0.3175(55)	0.3083(54)	0.3498(68)
0.1245	0.1230	0.2451(9)	0.2404(9)	0.4054(46)	0.2754(15)	0.3239(53)	0.3225(49)	0.3143(52)	0.3548(64)
0.1245	0.1235	0.2383(10)	0.2349(9)	0.4035(51)	0.2705(16)	0.3180(57)	0.3168(53)	0.3085(56)	0.3507(69)
0.1245	0.1240	0.2312(10)	0.2294(10)	0.4016(58)	0.2656(18)	0.3122(63)	0.3112(60)	0.3028(61)	0.3470(77)
0.1245	0.1245	0.2237(11)	0.2237(11)	0.4000(68)	0.2609(19)	0.3065(71)	0.3065(71)	0.2972(70)	0.3444(89)
fit range		28–56	28–56	16–24	28–58	26–44	26–44	26–44	26–44

TABLE VII: The same results as Table V for $\beta = 6.10$.

		Positive-parity baryons				Negative-parity baryons			
κ_1	κ_2	$m_{\text{oct}(\Sigma)}$	$m_{\text{oct}(\Lambda)}$	m_{sing}	m_{dec}	$m_{\text{oct}(\Sigma)}$	$m_{\text{oct}(\Lambda)}$	m_{sing}	m_{dec}
0.1230	0.1230	0.2382(4)	0.2382(4)	0.3466(30)	0.2560(7)	0.2967(23)	0.2967(23)	0.2925(20)	0.3103(26)
0.1230	0.1235	0.2320(5)	0.2329(5)	0.3417(32)	0.2511(08)	0.2911(25)	0.2919(25)	0.2875(21)	0.3059(28)
0.1230	0.1240	0.2257(5)	0.2276(5)	0.3365(35)	0.2463(08)	0.2854(27)	0.2874(27)	0.2827(22)	0.3017(32)
0.1230	0.1245	0.2193(5)	0.2223(5)	0.3311(39)	0.2417(09)	0.2796(29)	0.2835(33)	0.2783(25)	0.2981(38)
0.1235	0.1230	0.2271(5)	0.2262(5)	0.3370(35)	0.2462(8)	0.2867(26)	0.2858(26)	0.2826(22)	0.3014(31)
0.1235	0.1235	0.2208(5)	0.2208(5)	0.3325(38)	0.2413(09)	0.2809(28)	0.2809(28)	0.2776(24)	0.2969(34)
0.1235	0.1240	0.2143(5)	0.2154(5)	0.3277(42)	0.2365(10)	0.2750(31)	0.2762(31)	0.2728(26)	0.2926(38)
0.1235	0.1245	0.2076(6)	0.2101(6)	0.3226(48)	0.2319(11)	0.2689(34)	0.2722(38)	0.2683(29)	0.2889(46)
0.1240	0.1230	0.2160(5)	0.2137(5)	0.3268(42)	0.2366(10)	0.2768(32)	0.2746(31)	0.2729(26)	0.2929(39)
0.1240	0.1235	0.2095(6)	0.2082(5)	0.3232(47)	0.2317(11)	0.2709(34)	0.2695(34)	0.2680(28)	0.2883(43)
0.1240	0.1240	0.2028(6)	0.2028(6)	0.3193(53)	0.2270(12)	0.2646(37)	0.2646(37)	0.2631(31)	0.2840(49)
0.1240	0.1245	0.1958(6)	0.1974(6)	0.3150(62)	0.2225(13)	0.2581(42)	0.2604(45)	0.2586(35)	0.2803(59)
0.1245	0.1230	0.2049(6)	0.2006(6)	0.3151(55)	0.2276(12)	0.2680(44)	0.2628(42)	0.2638(33)	0.2855(56)
0.1245	0.1235	0.1982(7)	0.1950(6)	0.3133(63)	0.2228(14)	0.2617(48)	0.2575(45)	0.2588(36)	0.2809(63)
0.1245	0.1240	0.1912(7)	0.1894(7)	0.3114(74)	0.2182(15)	0.2551(53)	0.2523(50)	0.2540(40)	0.2765(72)
0.1245	0.1245	0.1839(8)	0.1839(8)	0.3094(91)	0.2139(18)	0.2479(61)	0.2479(61)	0.2493(46)	0.2727(88)
fit range		40–64	40–64	24–36	44–64	36–52	36–52	32–52	36–52

the same size (~ 2 fm), and we cannot examine the finite volume effects on these lattices. In Ref. [6], the finite volume effect on the negative-parity baryon masses was evaluated as 5% by comparing the masses on lattices with volume sizes 1.5fm and 2.2fm (1.6fm and 2.1fm) at $\beta = 6.0$ (6.2) on quenched isotropic lattices. This amount of fi-

nite size effect may also exist in our results, while our lattice volumes are close to the larger ones in Ref. [6].

- *Lattice discretization error*

Table VIII shows the baryon masses on each lattice. We find it hard to take the continuum limit even

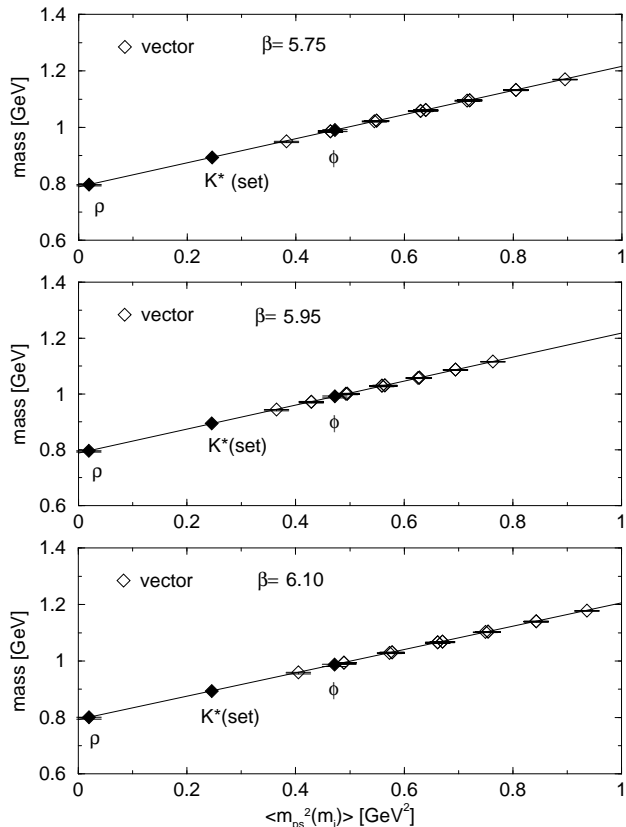


FIG. 2: The spectrum of the vector meson plotted against the pseudoscalar meson mass squared m_{ps}^2 in the physical unit. The open symbols denote the direct lattice data, and the filled symbols denote the results for the physical quark masses obtained from the lattice data with the linear chiral extrapolation.

for the ground-state baryons and mesons, since only the three β 's are taken here and their behavior is not so smooth that one can apply a simple extrapolation. In addition, such fluctuating behavior of data may be large due to the lack of statistics, genuine discretization errors would not be negligible. In the range of lattice cutoff 1–2 GeV, the fluctuation of masses is at most about 5%, except for the case of Λ_{sing}^+ for which 7% deviation is found. This gives us a hint on the potential size of the discretization errors. We also note that Ref. [23] examined how the $O(\alpha a)$ and $O(a^2)$ discretization effects decrease as β increases in the meson sectors, and found that those in the calibration of γ_F are sufficiently reduced already at $\beta = 6.10$. For these reason we discuss physical consequences of our result mainly based on the data of $\beta = 6.10$ lattice in the next section.

- *Chiral extrapolation*

From the study of the chiral perturbation theory, there appears a non-analyticity in the chiral extrap-

TABLE VIII: The Hadron spectrum expressed in the unit of GeV at the physical quark masses. The K^* meson mass is used for the determination of the scale unit a_τ .

	$\beta = 5.75$	$\beta = 5.95$	$\beta = 6.10$
ρ	0.7973(52)	0.7965(53)	0.8005(65)
K^*	0.8939	0.8939	0.8939
ϕ	0.9905(55)	0.9913(53)	0.9873(66)
N	1.1118(84)	1.0781(81)	1.1055(72)
Λ	1.2095(75)	1.1825(75)	1.2002(67)
Σ	1.2256(76)	1.1982(76)	1.2173(67)
Ξ	1.3393(71)	1.3183(75)	1.3291(67)
Δ	1.366(23)	1.342(16)	1.3685(17)
Σ^*	1.459(20)	1.440(14)	1.4586(15)
Ξ^*	1.552(17)	1.538(12)	1.5486(13)
Ω	1.645(15)	1.635(11)	1.6387(12)
$N^{(-)}$	1.686(79)	1.599(59)	1.618(57)
$\Sigma^{(-)}$	1.784(67)	1.705(49)	1.717(49)
$\Xi^{(-)}$	1.882(56)	1.810(40)	1.816(42)
$\Lambda_{\text{oct}}^{(-)}$	1.788(66)	1.703(48)	1.700(49)
$\Lambda_{\text{sing}}^{(-)}$	1.732(28)	1.646(49)	1.725(39)
$\Delta^{(-)}$	1.806(84)	1.877(73)	1.833(80)
$\Sigma^{*(-)}$	1.896(72)	1.955(61)	1.913(69)
$\Xi^{*(-)}$	1.986(60)	2.032(50)	1.994(57)
$\Omega^{(-)}$	2.077(49)	2.109(39)	2.074(46)
$\Lambda_{\text{sing}}^{(+)}$	2.288(58)	2.292(46)	2.150(70)

olation at the quenched level near the chiral limit as $m_\pi < 400$ MeV [27]. We have, however, taken the naive linear extrapolation for both the positive- and negative-parity baryons, because the results for the baryon masses seem to be well described with the linear relation in the quark-mass region corresponding to $m_\pi > 600$ MeV in the present calculation. In addition, the behavior of the negative-parity baryon masses near the chiral limit is less known. Therefore, it is difficult to estimate the non-analyticity in the chiral extrapolation from the present results. The quantitative estimate of its effect on the negative-parity baryon masses is a future problem with high precision data with small quark masses.

- *Quenching effects*

There is about 10% uncertainty for the ground-state hadron spectra coming from the quenching effect. Also for the negative-parity baryons, there should appear such a quenching effect. In addition, there may appear nontrivial excitation effect of the η' meson in quenched QCD, where η' degenerates with the other Nambu-Goldstone bosons in the chiral limit due to the ignorance of the fermionic determinant. Such an effect from η' is reported to appear near the chiral limit as $m_\pi < 300$ MeV [28].

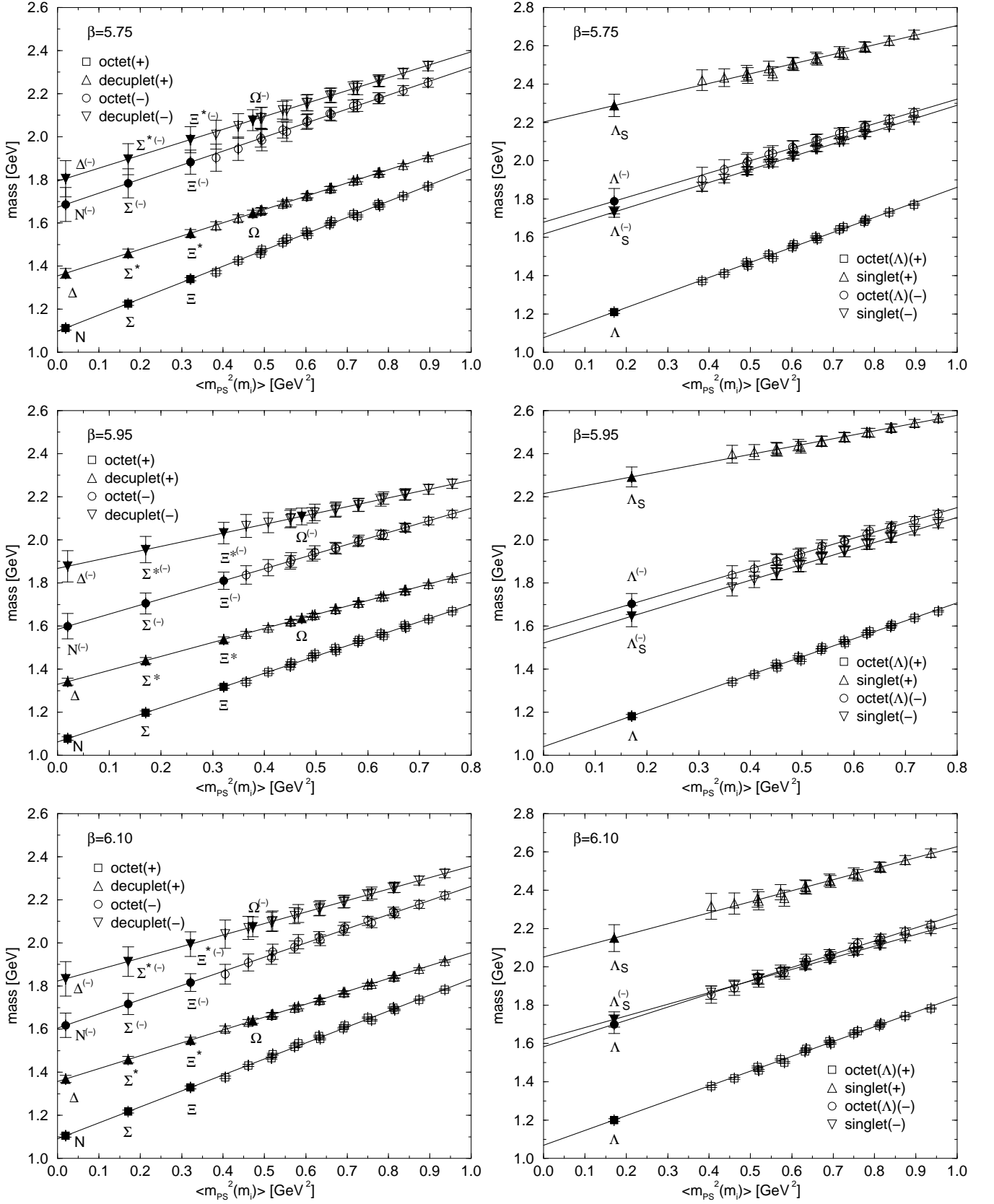


FIG. 3: The spectra of positive- and negative-parity baryons plotted against the pseudoscalar meson mass squared m_{PS}^2 . For each β , the octet and the decuplet baryons are shown in the left panel and octet(Λ) and singlet baryons in the right panel. The horizontal axis denotes the averaged pseudoscalar mass square. The open symbols denote the direct lattice data, and the filled symbols denote the results for the physical quark masses obtained from the lattice data with the linear chiral extrapolation.

IV. DISCUSSION

Our numerical results for the hadron spectra are summarized in Fig. 3 and Table VIII. The masses of the negative-parity baryons are found to be heavier than those of the corresponding positive-parity sectors, as expected. The flavor-singlet baryon is, however, an exception: the positive-parity baryon is much heavier than the negative-parity one. This tendency seems consistent with the 3Q state in the quark model, in which the flavor-singlet positive-parity baryon belongs to the 70-dimensional representation of the $SU(6)$ symmetry with the principal quantum number $N = 2$. This multiplet is in general heavier than that belonging to the negative-parity baryons. QCD sum rule analysis [29] and the other recent lattice calculation [7] also predict the mass of the flavor-singlet negative-parity baryon lighter than that of the positive one.

In order to compare our lattice results with experimental values, various baryon masses at $\beta = 6.10$ together with the experimental values are shown in Fig. 4. For the positive-parity baryons, the nucleon and the delta masses are somewhat higher than the experimental ones. Note again that quenched QCD exhibits the non-analytic behavior in the chiral extrapolation on the nucleon near the chiral limit of $m_\pi < 400$ MeV [27]. In comparison with the naive linear extrapolation, this effect lowers the nucleon mass in the chiral limit, although we have not taken into account the non-analytic behavior because of the absence of its signal in our relatively heavy quark-mass region of $m_\pi > 600$ MeV. The other positive-parity baryons with strangeness reproduce the experimentally observed masses within 10% deviations. The better reproduction of strange baryon masses may be natural because of the following reason. For the strange baryon, the ambiguity from the chiral extrapolation would be less than that of the nucleon and the delta, because the strange quark is relatively massive and the non-analytic behavior arises only from up and down quark mass region.

As for the negative-parity baryons, most of the present lattice results comparatively well reproduce the experimental spectra as shown in Fig. 4, in spite of a relatively large statistical error. However, the flavor-singlet negative-parity baryon is exceptional, and its calculated mass of about 1.7 GeV is much heavier than the experimentally observed $\Lambda(1405)$ with the difference of more than 300 MeV. The difference between the lattice result of 1.7 GeV and the experimental value of the $\Lambda(1405)$ is, however, the largest in all the hadrons in consideration. Even taking the quenching effect into account, this discrepancy seems too large. (Note again that the flavor-singlet baryon has one strange quark, and the ambiguity from the chiral extrapolation is expected to be less than that of the nucleon and the delta.)

If the $\Lambda(1405)$ could be well described as a three valence quark system, its mass would be reproduced with the simple three-quark operator in quenched QCD. However, the light mass of the $\Lambda(1405)$ is not reproduced

in the present simulation. Therefore, the present lattice QCD result physically indicates that the experimentally observed $\Lambda(1405)$ cannot be described with a simple three valence quark picture, that is, the overlap of the $\Lambda(1405)$ with the 3Q component is rather small. This seems to support other possible pictures for the $\Lambda(1405)$ such as the penta-quark state or the $N\bar{K}$ molecule. In this sense, lattice QCD simulations with the penta-quark operator would be meaningful to elucidate the nature of the $\Lambda(1405)$.

Here, we add several comments and cautions in quenched QCD. First, there is possible mixing between 3Q and 5Q states through the “Z-graph” even in the quenched approximation [30]. Therefore, to be strict, the separability into 3Q and 5Q states does not hold even in the quenched approximation, although the mixing between the two states is rather suppressed. Nevertheless, the conclusion of the non-3Q picture for the $\Lambda(1405)$ is still plausible, because, if the $\Lambda(1405)$ is described as the 3Q state, its mass is to be reproduced with the 3Q operator in quenched QCD. Second, for the definite conclusion, we have to pay attention to the non-analytic behavior in the flavor-singlet negative-parity baryon near the chiral limit [8], in spite of the naive expectation of its smaller effect for strange baryons. Third, according to the neglect of the fermionic determinant, η' becomes unphysically “light” as the Nambu-Goldstone particle in quenched QCD, and the non-unitary behavior appears in the baryon correlator due to the “light” η' excitation near the chiral limit below $m_\pi \sim 250$ MeV [28], where there appears an unphysical “decay” process of the negative-parity baryon into an η' -N state. Although these non-analytic and the non-unitary behaviors are not observed in the present simulation with relatively heavy quark masses as $m_\pi > 600$ MeV, these effects should be taken into account for the simulation near the chiral limit.

We now focus on other negative-parity baryons. The mass ratio between the positive- and the negative-parity baryons is shown in Table IX. For both the octet and the decuplet baryons, the relative mass difference between the parity partners becomes smaller, as the averaged quark mass increases by the inclusion of the strange quark. This tendency is experimentally observed for the octet baryons. (The empirical identification of negative-parity decuplet baryons is not established.) This behavior is also reported in another lattice QCD analysis by the domain wall fermion [5]. From Fig. 4 and Table IX, we find that the lattice results of the flavor octet and decuplet baryons are all close to the observed lowest-lying negative-parity baryons, the $N(1535)$, $\Lambda(1670)$, $\Sigma(1620)$ and $\Delta(1700)$, in spite of the relatively large statistical error. The $\Sigma(1620)$, which is experimentally confirmed as the negative-parity strange baryon with $J^P = 1/2^-$ [16], is consistent with the parity partner of the Σ baryon. The parity partner of the Ξ baryon is expected to be the $\Xi(1690)$ from our calculation, although the spin-parity of the $\Xi(1690)$ is not yet confirmed experimentally. Recently it has been proposed based on the chiral unitary

approach [31] that the $\Xi(1620)$ has the negative-parity, although its experimental status is still one-star (evidence of existence is poor). It is, however, difficult to distinguish between the $\Xi(1620)$ and the $\Xi(1690)$ from our result due to the statistical errors. For the decuplet baryons, we can regard the parity partner of the $\Delta(1232)$ as the $\Delta(1700)$, although the experimental data is poor. The positive-parity flavor-singlet baryon is found to be much heavier than the negative-parity decuplet, and hence its investigation seems much difficult both theoretically and experimentally.

Finally, we comment on recent lattice studies on the negative-parity baryons. Sasaki *et al.* investigated the negative-parity non-strange baryon $N^{(-)}$, the parity partner of the nucleon $N^{(+)}$, with the domain wall fermion [5]. Their lattice is $16^3 \times 32$ at $\beta = 6.0$ ($a^{-1} = 1.9$ GeV) and the result is $N^{(-)}/N^{(+)} \sim 1.45$, which is consistent with ours. Göckler *et al.* studied the negative-parity non-strange baryon $N^{(+)}$ using the $O(a)$ improved Wilson quark on the isotropic lattices with the size of $16^3 \times 32$ and $32^3 \times 64$ [6]. They obtained the similar result, $N^{(-)}/N^{(+)} = 1.50(3)$. Melnitchouk *et al.* also studied the negative-parity baryons using the $O(a)$ improved Wilson quark on the isotropic lattice, $16^3 \times 32$ ($a = 0.125$ fm) [7]. Since they did not carry out the chiral extrapolation, we do not compare the results quantitatively, but the qualitative behavior is similar to us. They also investigated the flavor-singlet baryons. Instead of the flavor-singlet interpolating field, they used the “common” interpolating field which is the common part of the interpolating fields for the octet Λ hyperon and the singlet baryon. The result is much heavier than the experimental value of the $\Lambda(1405)$ even for such an field. Lee *et al.* investigated the excited state baryons with the overlap fermion with the lattice $16^3 \times 28$ [8]. They employed the constrained curve fitting method for the mass fitting and obtained the baryon masses lower than those from the conventional fitting method. Thus, their results seem to be lower than ours and the other’s, while they did not carry out the chiral extrapolation. Dynamical quark simulation of excited-state baryons is also in progress [9]. As for the negative-parity nucleon, their present result is consistent with the quenched result within statistical errors.

V. SUMMARY AND CONCLUDING REMARKS

We have studied the mass spectra of the negative-parity baryons and the flavor-singlet baryons in quenched anisotropic lattice QCD. We have used three lattices of almost the same physical spatial volume of about $(2\text{fm})^3$ with the spatial cutoffs $a_\sigma^{-1} = 1\text{--}2$ GeV and the renormalized anisotropy $\xi = a_\sigma/a_\tau = 4$. We have adopted the standard Wilson plaquette gauge action and the $O(a)$ improved Wilson quark action at the tadpole-improved tree-level [23]. The positive- and negative-parity baryon masses are extracted with the parity projection from the

same baryon correlators based on the three valence quark picture.

For the flavor octet and decuplet negative-parity baryons, the calculated masses are close to the experimental values of corresponding lowest-lying negative-parity baryons. For several negative-parity baryons, our lattice data have suggested some predictions. For instance, $\Delta(1700)$ can be regarded as the parity partner of $\Delta(1232)$, and the $\Xi(1690)$ would be the parity partner of the Ξ baryon, although the spin-parity of the $\Xi(1690)$ is not yet confirmed experimentally.

As for the flavor-singlet negative-parity baryon, such a three-quark state has been found to lie around 1.7GeV , and has been much heavier than the $\Lambda(1405)$. Even considering the systematic errors, this difference of about 300 MeV seems too large. If the $\Lambda(1405)$ is described as a three valence-quark state, its mass would be reproduced in the present simulation. In fact, the present lattice result which cannot reproduce the $\Lambda(1405)$ physically implies that the $\Lambda(1405)$ is not described as the simple three quark picture, i.e., the overlap of the $\Lambda(1405)$ with the three-quark state is rather small. This seems to support an interesting picture of the penta-quark state or the $N\bar{K}$ molecule for the $\Lambda(1405)$. For more definite understanding of the $\Lambda(1405)$, it would be desired to perform lattice QCD simulations in terms of the $N\bar{K}$ molecule or the penta-quark state. Such a study is interesting even at the quenched level, where dynamical quark loop effect is absent and then the quark-level constitution of hadrons is clearer. As for the positive-parity flavor-singlet baryon, its calculated result is found to be much heavier than the negative-parity one, as is consistent with the quark models [10, 11] and the QCD sum rule analysis [29].

Very recently, LEPS Collaboration has experimentally observed the Θ^+ (or Z^+) baryon with $S = +1$ [32], which requires at least “five valence quarks” as $uudds$ and is physically identified as a “penta-quark system”. The comparison between the Θ^+ baryon and the $\Lambda(1405)$ may be useful to investigate the features of the penta-quark system. It is also interesting to investigate this type of a penta-quark system using lattice QCD simulation.

From aspect of the chiral symmetry, the parity partner should be degenerate if the symmetry is restored at finite temperature and/or density. It is interesting to see how the mass difference between the parity partners changes at finite temperature on the lattice. Several works on it are already reported for the screening mass of the nucleon [33] and they favor the parity degeneracy at the chiral phase transition. Recently based on the chiral effective theory such as the linear sigma model [34] and the chiral perturbation theory [35], two different assignments for the negative-parity baryons have been proposed: under the chiral transformation, the negative-parity baryon transforms in the same way as the positive-parity one in one scheme and in the opposite way in the other. These two assignments behave differently toward the chiral restoration. Therefore, it is interesting to study them from the quark degrees of freedom such as in lattice QCD

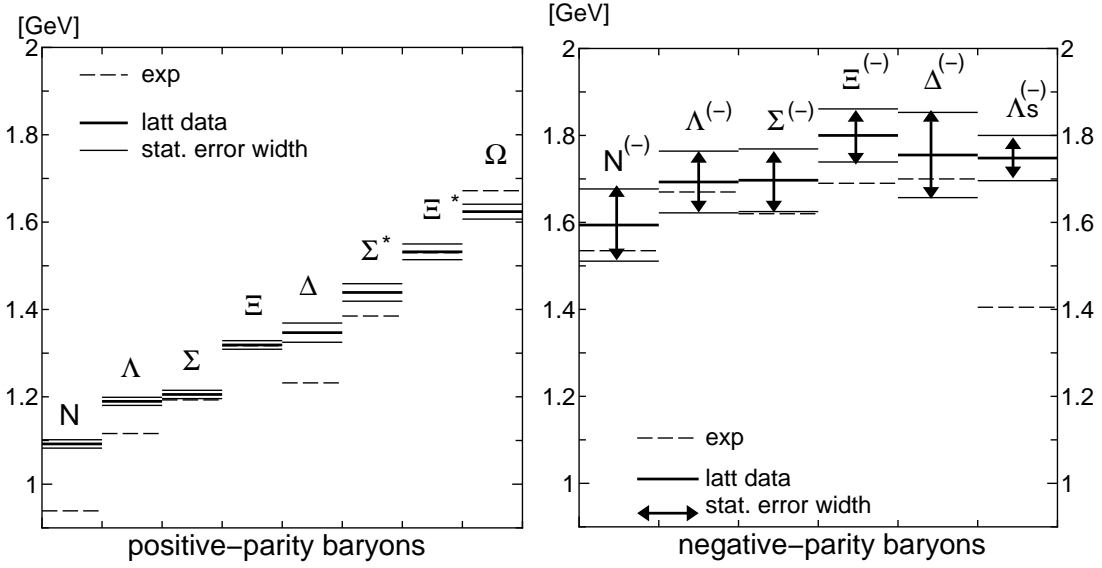


FIG. 4: Various baryon masses obtained from the $\beta = 6.10$ lattice. For the negative-parity baryons, the experimental values of $N(1535)$, $\Lambda(1670)$, $\Sigma(1620)$, $\Xi(1690)$, $\Delta(1700)$ and $\Lambda(1405)$ are added.

TABLE IX: The ratio of negative and positive-parity baryon masses. In the last line, the ratio of flavor-singlet negative-parity and octet positive-parity baryon masses is also listed. Physical values of the negative-parity baryons are taken to be $N(1535)$, $\Sigma(1620)$, $\Xi(1690)$, $\Lambda_{\text{oct}}(1670)$, $\Lambda_{\text{sing}}(1405)$ and $\Delta(1700)$. (*)Note that the spin-parity of the $\Xi(1690)$ is not yet confirmed.

	$\beta = 5.75$	$\beta = 5.95$	$\beta = 6.10$	physical value
$N^{(-)}/N^{(+)}$	1.516(70)	1.484(54)	1.463(51)	1.635
$\Sigma^{(-)}/\Sigma^{(+)}$	1.456(54)	1.423(40)	1.410(40)	1.358
$\Xi^{(-)}/\Xi^{+}$	1.405(41)	1.373(30)	1.366(31)	1.282*
$\Lambda_{\text{oct}}^{(-)}/\Lambda_{\text{oct}}^{(+)}$	1.479(54)	1.440(40)	1.417(40)	1.496
$\Lambda_{\text{sing}}^{(-)}/\Lambda_{\text{sing}}^{(+)}$	0.757(22)	0.718(26)	0.802(32)	
$\Delta^{(-)}/\Delta^{(+)}$	1.322(64)	1.399(55)	1.339(61)	1.380
$\Sigma^{*(-)}/\Sigma^{*(+)}$	1.299(52)	1.358(43)	1.312(49)	
$\Xi^{*(-)}/\Xi^{*(+)}$	1.280(41)	1.321(33)	1.288(38)	
$\Omega^{(-)}/\Omega^{(+)}$	1.263(31)	1.290(24)	1.266(29)	
$m_{\Lambda_{\text{sing}}^{(-)}}/m_{\Lambda_{\text{oct}}^{(+)}}$	1.432(23)	1.392(42)	1.437(34)	1.259

at finite temperature.

Acknowledgments

Y.N. thanks S. Sasaki, T. Blum and S. Ohta for useful discussions and comments. H.M. thanks T. Onogi and T. Umeda for useful discussions. The simulation was done on NEC SX-5 at Research Center for Nuclear Physics, Osaka University and Hitachi SR8000 at

KEK (High Energy Accelerator Research Organization). H.S. is supported in part by Grant for Scientific Research (No.12640274) from Ministry of Education, Culture, Science and Technology, Japan. H.M. is supported by Japan Society for the Promotion of Science for Young Scientists. Y.N. was supported by the center-of-excellence (COE) program at YITP, Kyoto University in most stage of this work and thanks RIKEN, Brookhaven National Laboratory and the U.S. Department of Energy for providing the facilities essential for the completion of this work.

[1] CP-PACS Collaboration, S. Aoki, G. Boyd, R. Burkhalter, S. Ejiri, M. Fukugita, S. Hashimoto, Y. Iwasaki, K. Kanaya, T. Kaneko, Y. Kuramashi, K. Nagai,

M. Okawa, H. P. Shanahan, A. Ukawa and T. Yoshie, Phys. Rev. Lett. **84**, 238 (2000).

[2] See for example for recent results, UKQCD colab-

- tion, C. R. Allton, S. P. Booth, K. C. Bowler, J. Garden, A. Hart, D. Hepburn, A. C. Irving, B. Joo, R. D. Kenway, C. M. Maynard, C. McNeile, C. Michael, S. M. Pickles, J. C. Sexton, K. J. Sharkey, Z. Sroczynski, M. Talevi, M. Teper and H. Wittig, Phys. Rev. D **65**, 054502 (2002); JLQCD collaboration, T. Kaneko, S. Aoki, R. Burkhalter, M. Fukugita, S. Hashimoto, K-I. Ishikawa, N. Ishizuka, Y. Iwasaki, K. Kanaya, Y. Kuramashi, M. Okawa, N. Tsutsui, A. Ukawa, N. Yamada and T. Yoshie, Nucl. Phys. B (Proc. Suppl.) **119**, 329 (2003).
- [3] N. Nakajima, H. Matsufuru, Y. Nemoto and H. Suganuma, AIP Conference Proceedings **CP594**, 349 (2001); H. Suganuma, N. Ishii, H. Matsufuru, Y. Nemoto and T.T. Takahashi, AIP Conference Proceedings **CP644**, 366 (2002); Y. Nemoto, N. Nakajima, H. Matsufuru and H. Suganuma, Nucl. Phys. **A721**, 879c (2003).
- [4] F. X. Lee and D.B. Leinweber, Nucl. Phys. B (Proc. Suppl.) **73**, 258 (1999).
- [5] S. Sasaki, T. Blum and S. Ohta, Phys. Rev. D **65**, 074503 (2002).
- [6] M. Göckeler, R. Horsley, D. Pleiter, P. E. L. Rakow, G. Schierholz, C. M. Maynard and D. G. Richards, Phys. Lett. B **532**, 63 (2002).
- [7] W. Melnitchouk, S. Bilson-Thompson, F. D. R. Bonnet, F. X. Lee, D. B. Leinweber, A. G. Williams, J. M. Zanotti and J. B. Zhang, Phys. Rev. D **67**, 114506 (2003).
- [8] F.X. Lee, S.J. Dong, T. Draper, I. Horvath, K.F. Liu, N. Mathur and J.B. Zhang, Nucl. Phys. B (Proc. Suppl.) **119**, 296 (2003).
- [9] UKQCD Collaboration, C.M. Maynard and LHP Collaboration, D.G. Richards, *hep-lat/0209165*. Nucl. Phys. B (Proc. Suppl.) **119**, 287 (2003).
- [10] N. Isgur and G. Karl, Phys. Rev. D **20**, 1191 (1979).
- [11] S. Capstick and N. Isgur, Phys. Rev. D **34**, 2809 (1986).
- [12] For recent review, see e.g. S. Capstick and W. Roberts, *nucl-th/0008028*.
- [13] T.T. Takahashi, H. Matsufuru, Y. Nemoto and H. Suganuma, Phys. Rev. Lett. **86**, 18 (2001); T.T. Takahashi, H. Matsufuru, Y. Nemoto and H. Suganuma, Phys. Rev. D **65**, 114509 (2002); T.T. Takahashi, H. Suganuma, H. Ichie, H. Matsufuru and Y. Nemoto Nucl. Phys. **A721**, 926c (2003).
- [14] H. Ichie, V. Bornyakov, T. Streuer and G. Schierholz, Nuclear Physics **A721**, 899c (2003).
- [15] T. T. Takahashi and H. Suganuma, Phys. Rev. Lett. **90**, 182001 (2003).
- [16] Particle Data Group, Phys. Rev. D **66**, 010001 (2002).
- [17] J.P. Liu, Z. Phys. C **22**, 171 (1984); S. Choe, Eur. Phys. J. A **3**, 65 (1998); S. Choe, Eur. Phys. J. A **7**, 441 (2000).
- [18] F. Karsch, Nucl. Phys. B **205**, 285 (1982).
- [19] N. Ishii, H. Suganuma and H. Matsufuru, Phys. Rev. D **66**, 014507 (2002); *ibid*, 094506 (2002).
- [20] T. Umeda, R. Katayama, O. Miyamura and H. Matsufuru, Int. J. Mod. Phys. A **16**, 2215 (2001).
- [21] QCD-TARO Collaboration, Ph. de Forcrand, M. Garcia Perez, T. Hashimoto, S. Hioki, H. Matsufuru, O. Miyamura, A. Nakamura, I.-O. Stamatescu, T. Takaishi and T. Umeda, Phys. Rev. D **63**, 054501 (2001); T. Umeda, K. Nomura and H. Matsufuru, *hep-lat/0211003*.
- [22] T. R. Klassen, Nucl. Phys. B **533**, 557 (1998).
- [23] H. Matsufuru, T. Onogi and T. Umeda, Phys. Rev. D **64**, 114503 (2001); T. Umeda, H. Matsufuru and T. Onogi, Nucl. Phys. B (Proc. Suppl.) **106**, 805 (2002).
- [24] J. Harada, A. S. Kronfeld, H. Matsufuru, N. Nakajima and T. Onogi, Phys. Rev. D **64**, 074501 (2001).
- [25] G. P. Lepage and P. B. Mackenzie, Phys. Rev. D **48**, 2250 (1993).
- [26] A. X. El-Khadra, A. S. Kronfeld and P. B. Mackenzie, Phys. Rev. D **55**, 3933 (1997).
- [27] D.B. Leinweber, A.W. Thomas, K. Tsushima and S.V. Wright, Phys. Rev. D **66**, 094507, (2000); J.N. Labrenz and S.R. Sharpe, Phys. Rev. D **54**, 4595 (1996).
- [28] S. J. Dong, T. Draper, I. Horvath, F. X. Lee, K. F. Liu, N. Mathur and J. B. Zhang, *hep-ph/0306199*.
- [29] D. Jido, N. Kodama and M. Oka, Phys. Rev. D **54**, 4532 (1996); D. Jido and M. Oka, *hep-ph/9611322*.
- [30] K. F. Liu, S. J. Dong, T. Draper, D. Leinweber, J. Sloan, W. Wilcox and R. M. Woloshyn, Phys. Rev. D **59**, 112001 (1999).
- [31] A. Ramos, E. Oset and C. Bennhold, Phys. Rev. Lett. **89**, 252001 (2002).
- [32] LEPS Collaboration (T. Nakano et al.), Phys. Rev. Lett. **91** 012002 (2003).
- [33] C. DeTar, J.B. Kogut, Phys. Rev. Lett. **59**, 399 (1987); Phys. Rev. D **36**, 2828 (1987); S. Gottlieb, W. Liu, D. Toussaint, R. L. Renken and R. L. Sugar, Phys. Rev. Lett. **59**, 1881 (1987); A. Gocksch, P. Rossi and U. M. Heller, Phys. Lett. B **205**, 334 (1988); K. D. Born, S. Gupta, A. Irbach, F. Karsch, E. Laermann, B. Petersson and H. Satz, Phys. Rev. Lett. **67**, 302 (1991); C. Bernard, M. C. Ogilvie, T. A. DeGrand, C. DeTar, S. Gottlieb, A. Krasnitz, R. L. Sugar and D. Toussaint, Phys. Rev. D **45**, 3854 (1992); S. Gottlieb, A. Krasnitz, U. M. Heller, A. D. Kennedy, J. B. Kogut, R. L. Renken, D. K. Sinclair, R. L. Sugar, D. Toussaint and K. C. Wang, Phys. Rev. D **47**, 3619 (1993); S. Gottlieb, U. M. Heller, A. D. Kennedy, S. Kim, J. B. Kogut, C. Liu, R. L. Renken, D. K. Sinclair, R. L. Sugar, D. Toussaint and K. C. Wang, Phys. Rev. D **55**, 6852 (1997).
- [34] D. Jido, Y. Nemoto, M. Oka and A. Hosaka, Nucl. Phys. A **671**, 471 (2000); D. Jido, M. Oka and A. Hosaka, Prog. Theor. Phys. **106**, 873 (2001).
- [35] Y. Nemoto, D. Jido, M. Oka and A. Hosaka, Phys. Rev. D **57**, 4124 (1998).